Catalysis Today 143 (2009) 179–186

Contents lists available at ScienceDirect

Catalysis Today

journal homepage: www.elsevier.com/locate/cattod

Nickel on lanthanum-modified γ-Al_2O_3 oxygen carrier for CLC: Reactivity and stability

Mohammad M. Hossain, David Lopez, Jose Herrera, Hugo I. de Lasa *

Chemical Reactor Engineering Center, Department of Chemical and Biochemical Engineering, The University of Western Ontario, London, ON, Canada N6A 5B9

ARTICLE INFO

Article history:
Available online 29 October 2008

Keywords:
CO_2 capture
CLC
Nickel-based oxygen carrier
La-modified γ-Al_2O_3

ABSTRACT

This study deals with the development of a lanthanum-modified Ni/La-γ-Al_2O_3 oxygen carrier suitable for a fluidized bed chemical-looping combustion (CLC) process. BET specific surface area analysis shows that the addition of La favors the thermal stability of γ-Al_2O_3 by preventing phase transformation. Temperature programmed characterization shows that the presence of La enhances the reducibility of the oxygen carrier by influencing the metal–support interactions helping the formation of reducible nickel species. Reactive characterization of the prepared oxygen carriers in a Chemical Reactor Engineering Center (CREC) fluidized Riser Simulator, using multiple reduction/oxidation cycles, demonstrates that the Ni/La-γ-Al_2O_3 particles display excellent reactivity and stability. The addition of La in the Ni/La-γ-Al_2O_3 influences the state of the surface minimizing the formation of nickel aluminate. It is argued that the addition of La also inhibits metal particle agglomeration by maintaining consistent metal dispersion during the cyclic oxidation/reduction processes.

© 2008 Elsevier B.V. All rights reserved.

1. Introduction

It is now widely accepted that the emission of greenhouse gases is the main contributor to global warming, and CO_2 is the most prevalent of these gas emissions. It is estimated that fossil fuel-based power generation contributes today to about one-third of the total carbon dioxide released from fuel combustion [1,2]. Thus, power generation via fossil fuel combustion with effective CO_2 capture has been considered as a way of drastically reducing CO_2 emission. However, the currently available CO_2 capture techniques are energy intensive and costly. In this regard, chemical-looping combustion (CLC) appears to have the potential for delivering a most efficient and low-cost technology [3,4].

CLC process is configured with two interconnected fluidized bed reactors: an air reactor and a fuel reactor (Fig. 1) and a solid oxygen carrier is circulated between the air and fuel reactors. In CLC, the fossil fuel is fed into the fuel reactor where it is oxidized by the lattice oxygen of the oxygen carrier. Complete combustion in the fuel reactor produces CO_2 and water vapor. Therefore, the CO_2 formed can be readily recovered by condensing water vapor, eliminating the need of an additional energy intensive CO_2 separation. The free-of-water CO_2 can be sequestrated or/and used for other applications. Once fuel oxidation completed the reduced metal oxide M_yO_{x-1} (or metal) is transported to the air reactor where it is re-oxidized and recycled back to the fuel reactor. In addition to CO_2 capture, CLC also minimizes NO_x formation since the fuel burns in the fuel reactor in an air-free environment and the reduced oxygen carrier is re-oxidized in the air reactor in the absence of a fuel, at comparatively lower temperatures [5].

The large-scale application of CLC is still contingent upon the availability of suitable oxygen carriers. For CLC, transition metal oxides such as NiO, CuO, CoO, Fe_2O_3 and Mn_2O_3 are considered as possible candidates for oxygen carrier [5]. The suitable metal oxides are deposited on an inert material such as SiO_2, TiO_2, ZrO_2, Al_2O_3 and YSZ (yttria-stabilized zirconia), in order to achieve fluidizabe characteristics of the carrier materials. In additions, the dispersed metal/metal oxide phases on the support material are less prone to agglomerate and able to maintain the reduction and oxidation activity of the oxygen carrier in repeated CLC cycles. Consequently, supported metal shows more stability, as compared to bulk metal oxides, and this when exposed to repeated high temperature CLC cycles. Recently, Hossain and de Lasa [6] reported the various oxygen carriers that have been studied in literature. Most of those articles studied Ni–NiO system due to its superior reactivity, negligible volatility at suitable CLC reactor conditions

* Corresponding author at: Chemical Reactor Engineering Center, Faculty of Engineering, Department of Chemical and Biochemical Engineering, The University of Western Ontario, London, ON, Canada N6A 5B9. Tel.: +1 519 661 2144; fax: +1 519 850 2931.
E-mail address: hdelasa@eng.uwo.ca (H.I. de Lasa).

0920-5861/$ – see front matter © 2008 Elsevier B.V. All rights reserved.
doi:10.1016/j.cattod.2008.09.006

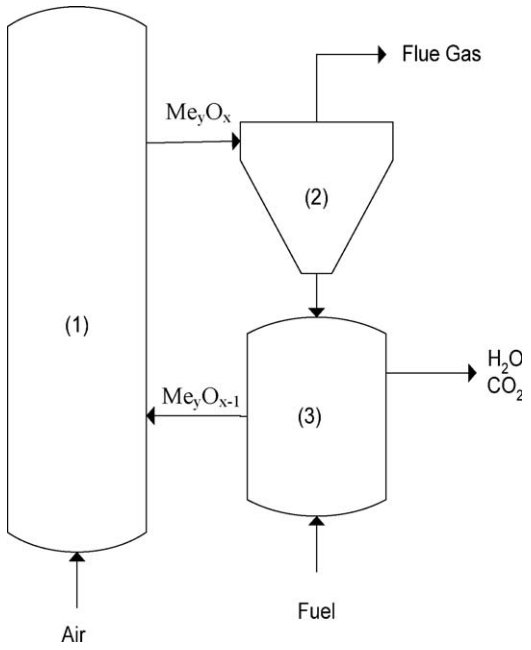

Fig. 1. Schematic view of chemical-looping combustion: (1) regenerator reactor, (2) cyclone and (3) fuel reactor.

[7–16]. Fe–Fe_2O_3-based materials were also found interesting as an oxygen carrier because of its wide availability and low price [17–20]. Cu–CuO is another oxygen carrier, which also displays encouraging reactivity and stability at lower temperature, i.e., 700 °C [13,21–23]. Due to its low melting point this carrier material is not suitable for high temperatures. Recently, Abad et al. [23] reported advantages, disadvantages and the range of operational conditions for Ni-, Fe- and Cu-based oxygen carriers.

A successful oxygen carrier should have high activity for both oxidation and reduction reactions, durability under repeated cycles, mechanical stability in fluidized bed reactor operation conditions and resistance to agglomeration in the fluidized bed reactors. In addition, the carrier must be economically feasible and environmentally sound [2,24–26]. At Chemical Reactor Engineering Center (CREC), The University of Western Ontario (UWO), the authors of this contribution have been working on developing a suitable oxygen carrier material with the above characteristics. To this end, a series of nickel-based oxygen carrier materials were synthesized, characterized and evaluated in mini-fluidized bed under CLC operating conditions. In oxygen carrier preparation γ-Al_2O_3 was used as support given its high surface area that provides higher metal dispersion as compared to α-Al_2O_3. Prior to nickel loading γ-Al_2O_3 was modified with La in order to achieve thermal stability of the support material. It has been reported that the additives based on rare-earth and/or alkaline-earth elements helps stabilizing γ-Al_2O_3 by preventing phase transformation at high working temperature [27,28].

This communication reports the effects of La on the Ni/La-γ-Al_2O_3 oxygen carrier using various characterization and evaluation methods. The thermal stability of the oxygen carrier was assessed by BET surface area analysis. Investigating temperature programmed reduction studies determined the reducibility of the prepared carrier material. The metal dispersion and metal crystal size was determined using pulse chemisorption. The reactivity and stability of the prepared oxygen carrier particles under repeated reduction/oxidation cycles was established using the CREC fluidized Riser Simulator using CH_4 and air for the respective cycles.

2. Experimental

2.1. Preparation of the modified alumina support and of the oxygen carrier

The oxygen carriers of the present study were prepared via an incipient wetness technique. With this end, 100 μm γ-Al_2O_3 particles with 233 m^2/g specific surface area were used as the support.

Prior to nickel loading the alumina support was modified adding La in order to improve its thermal stability. The amount of La was varied between 2 and 8 wt% and found optimum thermal stability can be achieved approximately 5 wt% La loading. Therefore, the oxygen carriers were prepared using 5 wt% La loaded γ-Al_2O_3 samples. Completed this 20 wt% nickel was added on a La-modified alumina support. Three main steps were involved in oxygen carrier preparation: support impregnation, reduction, and calcination. The highest limit (20 wt%) of nickel loading was selected aiming a possible higher amount of oxygen carrying capacity without any metal sintering or agglomeration [7,10].

Both for La-modified support or unmodified support Ni was loaded using the same methodology. The solutions were prepared by dissolving $Ni(NO_3)_2{\cdot}6H_2O$ or $La(NO_3)_3{\cdot}6H_2O$ powder in water. 0.8 mL of water was used for every gram of alumina support. During the impregnation step, aliquots of nitrate solution ($Ni(NO_3)_2{\cdot}6H_2O$) were introduced into the vacuum-sealed γ-Al_2O_3 under continuous mixing conditions. The resultant paste was dried slowly in a furnace by increasing the temperature form ambient to 140 °C over 6 h. The dried sample was then transferred to a specially designed fluidized bed reactor located in an oven contacting it with a flowing reducing gas mixture (10% hydrogen molar fraction basis and balanced helium). During oxygen carrier reduction phase, the bed temperature was raised from ambient to 750 °C over 4 h and maintained at 750 °C for 8 h. This thermal treatment decomposes nitrate ($Ni(NO_3)_2$) into oxides (NiO and/or $NiAl_2O_4$), reducing them further into their metallic form. Impregnation, calcinations and reduction steps were repeated until the desired metal loading was reached. Each cycle added 2.5 wt% nickel to the La-modified gamma alumina support. Once the desired metal loading was attained, the oxygen carrier was calcined in air and the oven temperature was raised from ambient to 750 °C using the same temperature ramp as used for reduction. Regarding nickel loading it is relevant to mention that the method adopted in this study provides a high degree of accuracy on achieving a specific metal loading target. Earlier, an SEM-EDX and ICP analysis of a 20% Ni on α-Al_2O_3 sample showed that the actual metal loading was within ±5% error band [10].

2.2. Nitrogen adsoprtion

The specific surface area, average pore radius and pore volume of the prepared oxygen carrier samples were determined in a Micromeritics ASAP 2010 analyzer by using N_2 adsorption at 77 K. For each experiment 0.1–0.2 g of sample was degassed at 573 K for 2.5 h before analysis. The adsorption isotherms were measured in 10^{-6}–1 relative pressure ranges. The total pore volume was determined from the amount of adsorption at a relative pressure close to unity. The average pore size was estimated assuming cylindrical pore geometry and by using the relation, D_p = (4 × pore volume/S_{BET}).

2.3. TPR/TPO, and pulse chemisorption characterization

Temperature programmed reduction (TPR), temperature programmed oxidation (TPO) and pulse chemisorption were con-

ducted in this study using a Micromeritics AutoChem II 2920 analyzer. A 100–200 mg of oxygen carrier sample was loaded in a U-shaped quartz reactor tube and this tube was placed into the sample port, located inside a heating element. The specifics of analysis are described in upcoming subsections.

2.3.1. TPR/TPO

TPR test was developed using a stream of gas containing 10% H_2 and 90% Ar circulated through a bed of the prepared oxygen carrier particles at a rate of 50 mL/min. Temperature was raised from ambient to 950 °C at a rate of 10 °C/min. A thermal conductivity detector (TCD) was used to analyze the gas leaving the bed. Hydrogen reacted with the oxide(s) with increasing the temperature. The TCD data was further processed to calculate the amount of hydrogen consumed during the reduction process. Finally, the amount of hydrogen consumed during TPR was used to calculate the number of reducible species as follows:

$$W_{Ni} = \frac{MW_{Ni} V_{H_2}}{\nu \rho_g} \quad (1)$$

where W_{Ni} represents the weight of reducible species, MW_{Ni} the molecular weight of reducible species, V_{H_2} the volume of hydrogen consumed at STP, ν the stoichiometric number based on the following reaction stoichiometry: $NiO + H_2 \rightarrow Ni + H_2O$ and ρ_g the gas molar volume at STP.

Furthermore, the percentage reduction can be calculated as follows:

$$\%\text{reduction} = \frac{W_{Ni}}{W_O} \times 100 \quad (2)$$

where W_{Ni} represents the weight of the reducible species and W_O the actual metal amount on the oxygen carrier.

TPO was conducted following each one of the TPR experiments. The procedure for TPO characterization began by flowing a stream of 5% O_2 and 95% He gas through a bed of oxygen carrier particles (now in its reduced form) at a rate of 50 mL/min. The bed temperature was increased from ambient to 950 °C at a rate of 10 °C/min and the TCD analyzed the gas in the exit stream.

2.3.2. Pulse chemisorption

Pulse chemisorption experiments were developed to determine active surface area, percent metal dispersion and active particle size. To perform a pulse chemisorption characterization, a stream of argon gas flowed through a bed of pre-reduced carrier at a rate of 50 mL/min. A series of hydrogen pulses (1.0 mL) were injected into the system at ambient temperature. A TCD detector analyzed the exit gas from the sample. As hydrogen gas was adsorbed by the sample, peaks were created in the TCD reading of the outlet stream. The pulse chemisorption was completed when two consecutive peaks had the same area.

The amount of hydrogen chemically adsorbed on the active sites of the oxygen carrier is used to calculate the percent dispersion (%D) as follows:

$$\%D = \frac{AX}{Wf} \quad (3)$$

where A represents a constant, X represents the total hydrogen chemisorbed, W represents the percentage of weight metal and f represents the fraction of reduced metal.

Furthermore, the average crystal size (d_v) is calculated as follows:

$$d_v = \frac{\varphi V_m}{S_m} \times \frac{1}{\%D} \quad (4)$$

where V_m represents the volume of metal atoms, φ represents the particle shape constant and S_m represents the average surface area of metal particles exposed per surface metal atom.

2.4. Reactive characterization in the CREC riser simulator

The reactivity and the regenerability of the prepared oxygen carriers was established using the CREC Riser Simulator under expected conditions (turbulent fluidized bed and temperature ranges between 600 and 750 °C) of an industrial scale fluidized CLC unit. The CREC Riser Simulator is a bench scale mini-fluidized bed reactor, invented at CREC-UWO [29]. This mini-fluidized reactor (volume of 50 cm^3) was designed for catalyst evaluation and kinetic studies under fluidized bed (riser/downer) reactor conditions. The CREC Riser Simulator consists of two sections: the upper shell and the lower shell. These shells allow easy access to the reactor to load and unload the oxygen carrier. An impeller, located in the upper section, and a basket containing the solid oxygen carrier, located in the central section, are the main components of the reactor. Upon rotation of the impeller at high speed (up to 7000 rpm), gas is forced both outward in the impeller section and downwards in the outer reactor annulus, causing the solids catalyst to become fully fluidized. A schematic diagram of the CREC-Riser Simulator, along with the gas injector and anemometer location, is illustrated in Fig. 2.

For each reaction experiment in the CREC Riser Simulator, 1 g of solid oxygen carrier was first loaded into the reactor basket and then the reactor was closed. A temperature programme was run to heat the system to the desired temperature (650 °C) for the combustion (carrier reduction) reaction. An argon flow was maintained during the heating period to ensure that the reactor system was free from oxygen (air). Once the reactor reached the desired pre-set temperature, the argon flow was arrested and the reactor was closed when it reached to 1 atm pressure. Finally, the vacuum box was brought to 20.7 kPa (3.0 psi) using a vacuum pump. At this stage the impeller was turned on and the feed (10 mL of CH_4) was injected into the reactor using a preloaded syringe. During this period of methane combustion, the pressure profile of the reactor was recorded using a pressure transducer. At the end of the pre-specified reaction time (40 s), a valve isolating the reactor and the vacuum bottle was opened and the contents of the reactor were transferred to the vacuum bottle. This introduced an abrupt decrease of the reactor pressure confirming that most of the reactant/product species were removed from the reactor almost instantaneously and that no further reaction took place. Finally, the product species were analyzed using a gas chromatograph. Before the next cycle, the oxygen carrier was regenerated (oxidized) by flowing air at a specified temperature and during a pre-set reaction time.

3. Results and discussions

3.1. Specific surface area

The specific surface area and pore volume determined by nitrogen physisorption for the support materials (γ-Al_2O_3 and La-modified La-γ-Al_2O_3) and Ni-loaded oxygen carriers are listed in Table 1. The 233 m^2/g BET surface area of the commercial γ-Al_2O_3 compared well with the value given by the supplier. After calcination at 750 °C for 8 h, the surface area of γ-Al_2O_3 was drastically decreased to 18 m^2/g. According to previous studies this sharp decrease in surface area is attributed to the thermal sintering of γ-Al_2O_3 via phase transformation towards θ-Al_2O_3 and α-Al_2O_3 phases [28]. The oxygen carrier calcined at 750 °C after nickel addition (Ni/γ-Al_2O_3), also showed a surface area reduction close

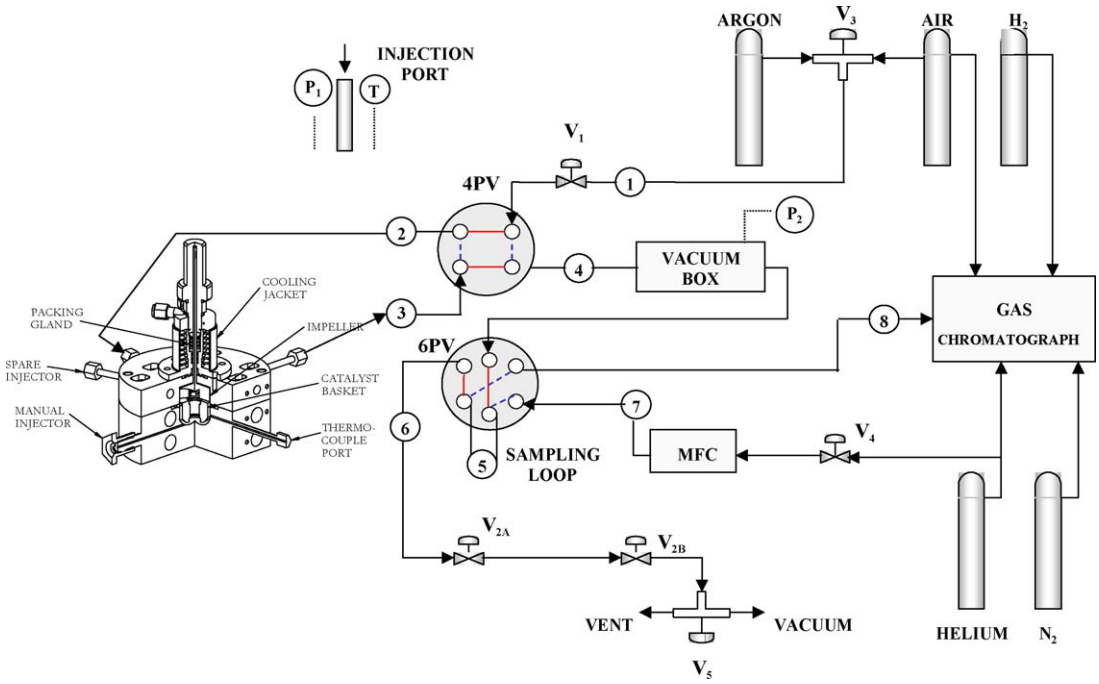

Fig. 2. Schematic diagram of the CREC Riser Simulator (quarter section view) experimental set up [29].

to the value of the bare calcined alumina support. This result indicates that loading of nickel did not affect the support with respect to the thermal stability. On the other hand, the La-modified La-γ-Al_2O_3 support displayed a marked enhancement of in the specific surface area over the values obtained for a bare and nickel-loaded γ-Al_2O_3 sample. Therefore the addition of La into the γ-Al_2O_3 significantly improves the thermal stability of the γ-Al_2O_3. This improvement in the thermal resistance of γ-Al_2O_3 demonstrates that La inhibits the transformation of γ-Al_2O_3 into low surface area θ-Al_2O_3 and α-Al_2O_3 phases [27,28]. On the other hand when nickel was loaded on the La-modified La-γ-Al_2O_3 support its specific surface area was slightly reduced to 112 m^2/g. This stabilized specific surface area show that impregnated nickel did not presumably affect the available pores of the support material, i.e., pore volume of the samples remained unchanged before and after metal loading (Table 1). Thus, the loaded nickel was mainly dispersed on the surface of the La-modified support and the area reduction due to the metal dispersion is counterbalanced by the dispersed nickel particles.

3.2. Temperature programmed studies

In CLC, the solid oxygen carrier undergoes repeated reduction–oxidation cycles. Therefore, a most important characteristic of an oxygen carrier is its reactivity and stability under cyclic operation. To investigate these matters, successive TPR and TPO experiments were developed.

Table 1
BET surface area and pore of support and oxygen carrier samples.

Sample	BET surface area (m^2/g)	Pore volume (cm^3/g)
γ-Al_2O_3 (as received)	233	0.253
γ-Al_2O_3 (calcined @ 750 °C)	18	0.103
La-γ-Al_2O_3 (calcined @ 750 °C)	113	0.295
Ni/γ-Al_2O_3 (calcined @ 750 °C)	17	0.101
Ni/La-γ-Al_2O_3 (calcined @ 750 °C)	112	0.295

TPR is also very effective for determining the reducibility (the temperature at which the reduction occurs and the percentage of reduction), of the oxygen carrier as well as for assessing the number of reducible species available in the oxygen carrier. Exposure to repeated reduction/oxidation cycles can cause a loss in oxygen carrier activity due to metal–support interactions resulting in the formation of non-reducible species. Thus, cyclic TPR/TPO characterization shows both reactivity losses due to metal–support interaction and agglomeration of the nickel crystallites.

Fig. 3 reports TPR profiles of the prepared oxygen carrier samples with the temperature being ramped (10 °C) from 30 °C to 950 °C. A TPR profile for La-γ-Al_2O_3 is also included as a reference. For the La-γ-Al_2O_3 no TPR peak is observed with the hydrogen consumed being negligible. It is believed that during the preparation steps La interact with γ-Al_2O_3 to form $LaAlO_3$ perovskite aluminate, which is difficult to reduce even at 950 °C

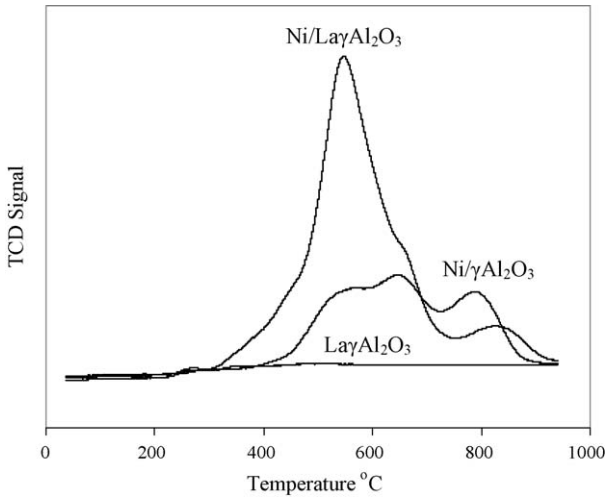

Fig. 3. TPR profiles of (a) La-γ-Al_2O_3, (b) Ni/γ-Al_2O_3 and (c) Ni/La-γ-Al_2O_3 samples (heating rate: 10 °C/min; reducing agent: 10 mol% H_2, balanced Ar at 50 cm^3/min).

[30]. The reduction profile of Ni/γ-Al_2O_3 shows a large wide asymmetric TPR peak from 400 °C to 750 °C. This broad peak displays a maximum at 650 °C. The tail on the TPR peak is an indication that metal species reduction takes place at temperatures higher than 650 °C. This TPR suggests that more than one species contributes to the overall Ni/γ-Al_2O_3 reduction.

According to Richardson et al. [31] NiO and $NiAl_2O_4$ are reducible phases in the 325–700 °C range, with the species reduced above 600 °C being nickel aluminate. As seen in Fig. 3, a small peak also appears between 750 and 900 °C. This peak is assigned to the reduction of pure $NiAl_2O_4$.

Rynkowski et al. [32] reported similar nickel oxide formation in a Ni-alumina catalyst system applicable for methane reforming. Using TPR and X-ray diffraction studies, these authors concluded that the amorphous NiO supported on alumina and a spinel of $NiAl_2O_4$ differs in reducibility. $NiAl_2O_4$ is formed when nickel interacts with the alumina support. Reduction of the NiO species in the amorphous phase occurs in the temperature range of 380–690 °C. The reduction of $NiAl_2O_4$ occurs at temperatures above 780 °C. Jin et al. [33] investigated Ni on Al_2O_3 oxygen carriers suitable for CLC. XRD results show formation of $NiAl_2O_4$, resulting in low reduction conversions due to the decreased amount of available metal oxide, with nickel aluminate being stable up to 900 °C.

Moreover, concerning the La-modified Ni/La-γ-Al_2O_3 oxygen carrier its reduction gave a single, symmetric and comparatively narrow peak at 580 °C. A very small peak was also observed at 850 °C. The first peak is assigned to the reduction of the dominant metal phase, mainly NiO, while the second peak is due to the reduction of a small amount of nickel aluminate. XRD analysis also identified the presence of NiO and $NiAl_2O_4$ phases on both the Ni/γ-Al_2O_3 and Ni/La-γ-Al_2O_3 samples (Fig. 4), with no lanthanum-containing phase detected in the La-modified sample. This further confirms that La only helps to enhance the reducibility of Ni species, not being included in the crystalline phase. One can also notice that the combined TPR areas of the Ni/La-γ-Al_2O_3 are larger than the ones for the Ni/γ-Al_2O_3. This shows a higher degree of reducibility of the La-modified oxygen carrier. Other important observation for the La-modified sample is given by the shift of the 100 °C TPR peak towards lower temperatures, a clear indication of the higher reactivity of the Ni/La-γ-Al_2O_3 sample.

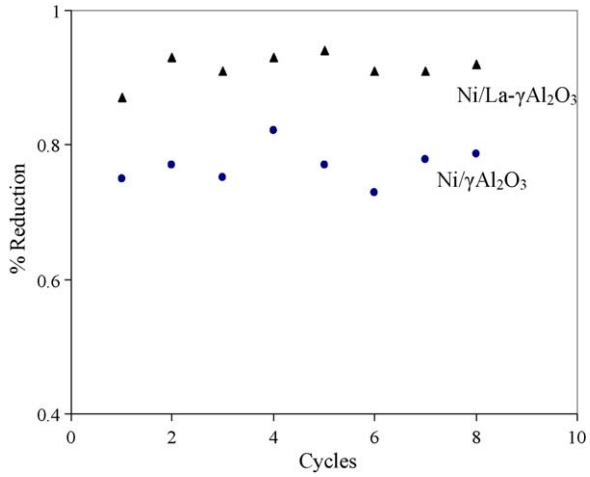

Fig. 5. Percentage reduction of nickel for Ni/γ-Al_2O_3 and Ni/La-γ-Al_2O_3 sample over repeated TPR/TPO cycles (heating rate: 10 °C/min; reducing agent: 10 mol% H_2, balanced Ar at 50 cm^3/min).

The effect of the number of reduction and oxidation cycles on reducibility of the nickel particles was also assessed from the cyclic TPR/TPO experiments. Each cycle was composed of TPR, pulse chemisorption and TPO. Multiple cycles were performed on both an unmodified Ni/γ-Al_2O_3 and a La-modified Ni/La-γ-Al_2O_3 oxygen carrier samples.

Fig. 5 compares the reducibility of the sample under repeated TPR/TPO cycles. As it can be noticed in Fig. 5 approximately 93% nickel conversion was achieved using the La-modified sample, with the highest nickel conversion remaining in the 76% range for the unmodified carrier. For both of the samples, the sequence of TPR/TPO cycles demonstrates consistent percentage reduction of nickel, indicating that the samples are stable over repeated reduction–oxidation cycles. This observation suggests that no phase transformation takes place during the repeated cyclic redox process. Therefore, a significant improvement of the oxygen carrying capacity was observed using the Ni/La-γ-Al_2O_3 oxygen carrier, with the addition of La helping the formation of easily reducible nickel oxide species minimizing nickel support interaction and formation of non-reactive nickel aluminates.

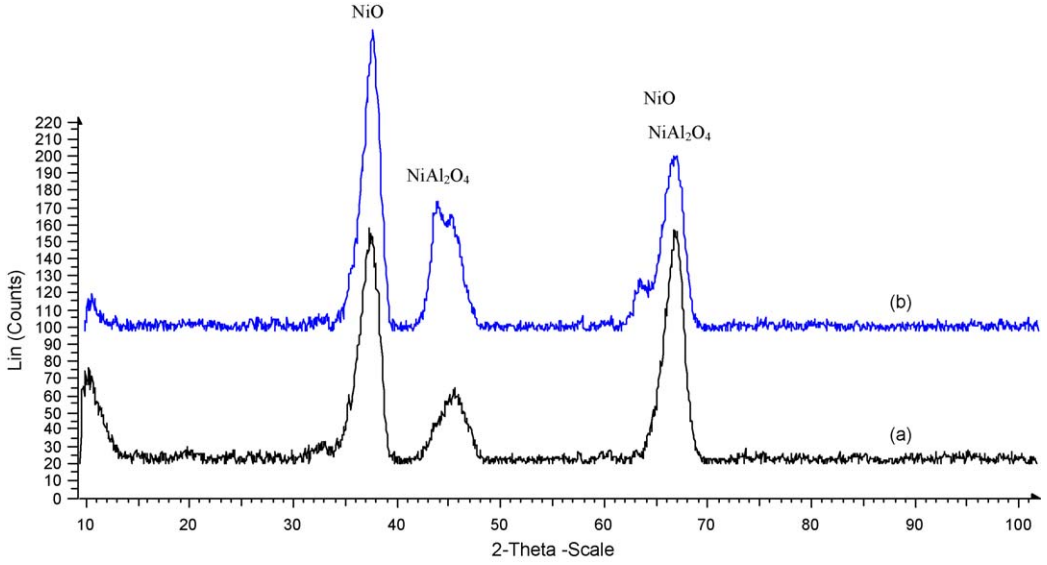

Fig. 4. XRD spectrum of (a) Ni/γ-Al_2O_3 and (b) Ni/La-γ-Al_2O_3 oxygen carriers.

The hydrogen pulse chemisorption results further confirmed the stable behavior of the sample in consecutive reduction and oxidation cycles (Table 2). Although both unmodified and modified samples showed a stable metal dispersion with successive reduction/oxidation cycles, a higher dispersion was observed in the modified sample versus the unpromoted sample: from 2.5% to 0.9%. This shows that La helps to increase the dispersion of nickel. Thus, it appears that addition of La alters the metal surface modifying the degree of interaction between Ni and alumina support while maintaining a consistent metal dispersion during the successive oxidations and reductions. It is also apparent that the metal crystal size of this bimetallic sample did not increase over repeated reduction/oxidation cycles, an indication of the absence of metal sintering (metal crystallite agglomeration).

3.3. CREC riser simulator studies

The reactivity and stability of both the unmodified and La-modified Ni/γ-Al_2O_3 oxygen carrier was analyzed in the CREC fluidized Riser Simulator using methane and air for the combustion and regeneration cycles, respectively. The combustion reaction was carried out at 650 °C and atmospheric pressure while the carrier re-oxidation was conducted at 575 °C and atmospheric pressure. The length of the fuel combustion cycles was 40 s. Complete re-oxidation of the reduced oxygen carrier was achieved under airflow for 10 min.

Generally a high temperature (1000–1200 °C) is preferable for the down stream turbine operations of a power generation processes. However, these conditions may lead to formation of NO_x in the oxidizer reactor and one of the main claimed advantages of CLC to eliminate NO_x formation may not be realized. A high reaction also causes the metal sintering and particle agglomeration, both phenomena having strong detrimental effects on the supported oxygen carrier activity [34]. Thus, there is significant potential and implementation value to consider the CLC in a lower temperature range, as in the present study, restricting the evaluation of the oxygen carriers to temperatures below 950 °C (the highest temperature level used for TPR/TPO experiments).

Using the experiments developed in the CREC Riser Simulator, one can notice, that the reduction for both the unpromoted and the La-promoted oxygen carrier is similar, with methane reacting rapidly forming CO_2 and H_2O. The upper curve of Fig. 6 displays a typical pressure profile during methane combustion in the CREC Riser Simulator, showing an increase in total pressure from injection to termination and this is due to the increase in the number of moles upon reaction between methane and the solid oxygen carrier. The lower curve represents the pressure profile of the vacuum box, which remained constant during the reaction. At termination point the reactor pressure is abruptly decreased to vacuum box pressure and the vacuum box pressure is slightly increased showing the transfer of gas from reactor to the vacuum box.

The gas chromatographic analysis of the gases contained in the CREC Riser Simulator vacuum box shows both CO_2 and H_2O, as major species of the methane combustion. The product analysis also displayed trace amounts of H_2; with no CO being detected in the combustion product gas sample.

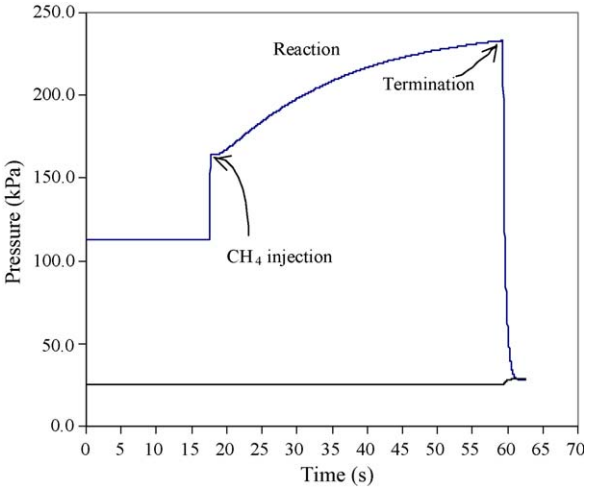

Fig. 6. Pressure profile in the CREC Riser Simulator for methane combustion with oxide particles (*T*: 650 °C; *P*: 1 atm).

From this observation, it is assumed that the combustion of methane with the nickel-based oxygen carriers (both unmodified and La-modified) proceeds according to the following reactions:

Combustion:

$$4NiO + CH_4 \leftrightarrow 4Ni + CO_2 + 2H_2O$$

$$4NiAl_2O_4 + CH_4 \leftrightarrow 4Ni + 4Al_2O_3 + CO_2 + 2H_2O$$

Decomposition:

$$CH_4 \rightarrow C + 2H_2$$

Reforming:

$$CH_4 + H_2O \leftrightarrow CO + 3H_2$$

$$CH_4 + CO_2 \leftrightarrow 2CO + 2H_2$$

Reduction with H_2:

$$H_2 + NiO \rightarrow Ni + H_2O$$

Reduction with CO:

$$CO + NiO \rightarrow Ni + CO_2$$

Water gas shift:

$$CO + H_2O \leftrightarrow CO_2 + H_2$$

The presence of trace amounts of H_2 in the product gas indicates the occurrence of some methane decomposition and reforming. Furthermore, H_2 formation via methane decomposition was confirmed by product analysis during the oxygen carrier

Table 2
Stability of oxygen carrier (reduction, dispersion, crystal size) over TPR/TPO cycles.

Sample		Reduction/re-oxidation cycles							
		1	2	3	4	5	6	7	8
Ni/γ-Al_2O_3	Dispersion (%)	0.75	0.90	0.88	0.96	0.90	0.78	0.92	0.91
	Crystal size (nm)	134.8	111.5	114.2	105.1	112.4	128.6	109.6	110.7
Ni/La-γ-Al_2O_3	Dispersion (%)	1.95	2.48	2.41	2.60	2.30	2.37	2.54	2.55
	Crystal size (nm)	49.7	39.2	40.2	37.2	47.6	38.1	38.2	38.0

regeneration cycle. Discussion of this matter is addressed in the upcoming paragraphs.

Product selectivity during methane combustion with a supported metal oxide is mainly associated with the degree of the reduction of the oxygen carrier [7,33]. At the beginning of the reaction (or short contact time), the fully oxidized oxygen carrier favors the total oxidation of methane to form CO_2 and H_2O. As the reaction proceeds, the partially reduced oxygen carrier also catalyzes the reforming reactions producing synthesis gas ($CO + H_2$). It is equally important to point out that both CO and H_2 are very reactive with the metal oxide under the studied reaction conditions being quickly converted to CO_2 and H_2O, respectively. Therefore, it can be assumed that the CO and H_2 produced via reforming reactions are further oxidized forming CO_2 and H_2O. Consequently and on the basis of this mechanistic interpretation it is possible to explain the absence of CO as a product of methane combustion while using the oxygen carriers of the present study.

On the other hand, oxygen carrier regeneration can be described with the following set of reactions:

Regeneration cycle

$$2Ni + O_2 \rightarrow 2NiO$$

$$2Ni + 2Al_2O_3 + O_2 \rightarrow 2NiAl_2O_4$$

$$C + O_2 \rightarrow CO_2$$

Thus, in the regeneration cycle, deposited carbon may lead to CO or/and CO_2 formation. One has thus, to minimize carbon formation to attain high CO_2 capture efficiencies. In the present study, the outlet gas analysis from the carrier re-oxidation cycle (regeneration) showed negligible amounts of CO and/or CO_2, with this being an indicator of little carbon formation during the reduction cycle and of the high performance of the oxygen carrier under study.

Regarding carbon formation, it is acknowledged that reaction times during the fuel combustion cycle may play a crucial role [33]. In this respect, reaction times selected for reaction testing in the CREC Riser Simulator were restricted to 40 s and this to prevent methane decomposition.

Methane and nickel oxide conversions were two important parameters assessed in the present study, with these two parameters defined as follows:

(i) Methane conversion was calculated from the product analysis data using Eq. (3), since CO_2 is the only carbon-bearing component in the methane combustion product,

$$X_{CH_4} = \frac{C_{CO_2,out}}{C_{CH_4,out} + C_{CO_2,out}} \times 100 \quad (5)$$

where $C_{CH_4,out}$ and $C_{CO_2,out}$ are the final concentrations of methane and carbon dioxide, respectively, remaining in the reactor after the desired reaction time. These concentrations of methane and carbon dioxide in the reactor were determined through gas chromatography of the product gases.

(ii) Nickel oxide(s) conversion was calculated on the basis of the number of moles of reacted oxygen, the weight of the carrier and the nickel composition of the carrier.

Nickel oxide conversion was then calculated:

$$X_{NiO} = \frac{4 \times N_{CH_4o} \times X_{CH_4}}{(w \times X_{W,NiO})/MW_{NiO}} \times 100 \quad (6)$$

where N_{CH_4o} is the initial number of moles injected into the reactor, X_{CH_4} is the conversion of methane, w is the mass of oxygen carrier loaded into the reactor, $X_{W,NiO}$ is fraction of nickel oxide present in the oxygen carrier sample and MW_{NiO} is the molecular weight of nickel oxide.

Fig. 7 displays the methane and oxygen carrier conversion during the combustion cycle for various reaction times. As it can be noticed in Fig. 7, approximately 91% methane conversion was observed with the La-modified oxygen carrier sample, with the highest methane conversion remaining in the 50% for the unmodified oxygen carrier. Therefore, a significant improvement of methane conversion was observed using the La-modified sample. The blank runs were developed for confirmation that both combustion and re-oxidation (650 and 575 °C, respectively) were adequate, with these blank runs showing a very low conversion in all cases (Fig. 7).

In CLC fuel conversion cycle, it is highly desirable that complete combustion of methane be achieved. The higher operating temperature is also favorable given higher reactor temperatures lead to a higher inlet temperature to the downstream gas turbine and as a result increased efficiency. However, the high reaction temperature also accelerates the formation of nickel aluminate, which is difficult to reduce/oxidize. To avoid metal sintering, researchers recommend the use of two fluidized bed reactors for fuel combustion instead of one in order to maintain a relatively low operating temperature. In this process configuration, the outlet gas from the first fluidized bed reactor enters the second fluidized bed reactor where the unreacted methane is combusted completely with fresh oxygen carrier [33]. This two fluidized bed concept could likely be also considered for bimetallic oxygen carriers such as the one of the present study.

The conversion of the oxygen carrier during the combustion reaction was calculated over repeated CLC cycles using the methane conversion data and Eq. (4), as shown in Fig. 8. For comparison the conversion of an alpha alumina-supported nickel oxygen carrier was also included in Fig. 8. For all the oxygen carrier samples tested, the sequence of CLC cycles performed demonstrates a consistent particle conversion, indicating that the oxygen carrier is stable over repeated CLC cycles.

At a reaction temperature of 650 °C, Ni in the NiO would be the only reduced species, as shown by TPR. Any $NiAl_2O_4$ formed through metal–support interaction would require a higher reduction temperature. These data is consistent with the results of Mattisson et al. [24] who reported that the alumina-supported nickel oxygen carrier was stable over multiple oxidation–reduction cycles in a

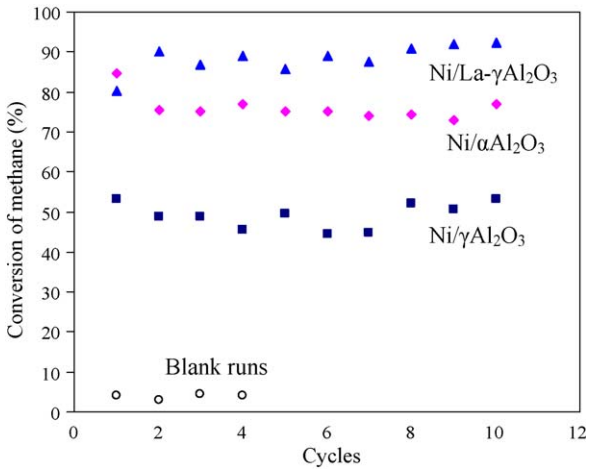

Fig. 7. Conversion of methane during multiple CLC cycles in CREC fluidized bed Riser Simulator (T: 650 °C; P: 1 atm). *Note*: repeated cycles were reproducible within ±3.5% standard deviation.

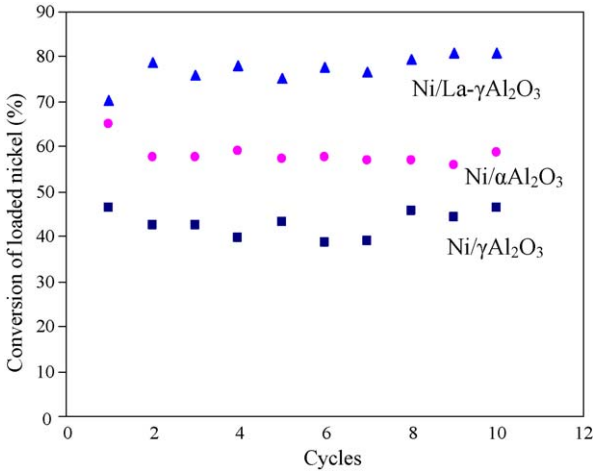

Fig. 8. Conversion of oxygen carriers in multiple CLC cycles in CREC fluidized bed Riser Simulator (*T*: 650 °C; *P*: 1 atm). *Note*: repeated cycles were reproducible within ±3.5% standard deviation.

thermogravimetric analyzer (TGA) at 750, 850 and 950 °C using a 10% CH_4, 10% H_2O, 5% CO_2 and 75% N_2 gas reducing mixture and 10% O_2 in N_2 for oxygen carrier regeneration.

These findings also agree with the results obtained using both TPR and TPO characterization methods of the present study, which showed that the Ni/γ-Al_2O_3 and Ni/La-γ-Al_2O_3 oxygen carrier are stable over multiple reduction–oxidation cycles. As it can be noticed in Fig. 8, average 80% nickel conversion was achieved using the La-modified sample while the highest nickel conversion remaining in the 50% range for the unmodified carrier.

4. Conclusions

The following are the conclusions of the present study:

(i) Nitrogen adsorption studies showed that the addition of La enhances the stability of γ-Al_2O_3 by maintaining its pore structures.

(ii) TPR/TPO results revealed that the presence of La to the alumina support increased the reducibility of the oxygen carrier by helping formation of NiO.

(iii) Pulse chemisorption demonstrates that La can provide better metal dispersion/re-dispersion. It is hypothesized that La interacts more readily with the alumina support, inhibiting the nickel aluminate formation.

(iv) Reactive characterization in a fluidized bed CREC Riser Simulator shows that during multiple reduction/oxidation cycles with CH_4 and air, the Ni/La-γ-Al_2O_3 display excellent reactivity and stability.

Acknowledgement

The authors would like to thank Natural Science and Engineering Research Council (NSERC) of Canada for financial support to this project.

References

[1] M. Halmann, M. Steinberg, Greenhouse Gas Carbon Dioxide Mitigation: Science and Technology, Lewis Publishers, Boca Raton, FL, USA, 2000.
[2] A. Lyngfelt, B. Leckner, T. Mattisson, Chem. Eng. Sci. 56 (2001) 3101.
[3] H.J. Richter, K.F. Knoche, ACS Symposium Series, 1983, p. 235.
[4] M. Ishida, D. Zheng, T. Akehata, Energy 12 (1987) 147.
[5] M. Ishida, H. Jin, Ind. Eng. Chem. Res. 35 (1996) 2469.
[6] M.M. Hossain, H.I. de Lasa, Chem. Eng. Sci. 63 (2008) 4433.
[7] M.M. Hossain, H.I. de Lasa, AIChE J. 53 (2007) 1817.
[8] M.M. Hossain, K.E. Sedor, H.I. de Lasa, Chem. Eng. Sci. 62 (2007) 5464.
[9] K.E. Sedor, M.M. Hossain, H.I. de Lasa, Can. J. Chem. Eng. 86 (2008) 323.
[10] K.E. Sedor, M.M. Hossain, H.I. de Lasa, Chem. Eng. Sci. 63 (2008) 2994.
[11] S.R. Son, S.D. Kim, Ind. Eng. Chem. Res. 45 (2006) 2689.
[12] J.E. Readman, A. Olafsen, J.B. Smith, R. Blom, Energy Fuels 20 (2006) 1382.
[13] Q. Zafar, T. Mattisson, B. Gevert, Energy Fuels 20 (2006) 34.
[14] E. Johanssson, T. Mattisson, A. Lyngfelt, H. Thunman, Fuel 85 (2006) 1428.
[15] T. Mattisson, M. Johansson, A. Lyngfelt, Fuel 85 (2006) 736.
[16] B.M. Corbella, L.F. de Diego, F. Gracia-Labiano, J. Adanez, J.M. Palacios, Ind. Eng. Chem. Res. 45 (2006) 157.
[17] M. Ishida, K. Takeshita, K. Suzuki, T. Ohba, Energy Fuels 19 (2005) 2514.
[18] F. Garcia-Labiano, J. Adanez, L.F. de Diego, P. Gayan, A. Abad, Energy Fuels 20 (2006) 26.
[20] B.M. Corbella, J.M. Palacios, Fuel 86 (2007) 113.
[21] B.M. Corbella, L.F. de Diego, F. Gracia-Labiano, J. Adanez, J.M. Palacios, Energy Fuels 19 (2005) 433.
[22] L.F. de Diego, P. Gayan, F. Gracia-Labiano, J. Celaya, A. Abad, J. Adanez, Energy Fuels 19 (2005) 1850.
[23] A. Abad, J. Adanez, F. Gracia-Labiano, L.F. de Diego, P. Gayan, J. Celaya, Chem. Eng. Sci. 62 (2007) 533.
[24] T. Mattisson, M. Johansson, A. Lyngfelt, Energy Fuels 18 (2004) 628.
[25] J. Adanez, L.F. de Diego, F. Garcia-Labiano, P. Gayan, A. Abad, Energy Fuels 18 (2004) 371.
[26] P. Cho, T. Mattisson, A. Lyngfelt, Fuel 83 (2004) 1245.
[27] R.M. Navarro, M.C. Álvarez-Galván, F. Rosa, J.L.G. Fierro, Appl. Catal. A: Gen. 297 (2006) 60.
[28] M.C. Álvarez-Galván, R.M. Navarro, F. Rosa, Y. Briceño, Hydrogen Energy 33 (2008) 652.
[29] H.I. de Lasa, US Patent 5,102,628 (1992).
[30] R. Blom, I.M. Dahl, Å. Slagtern, B. Sortland, A. Spjelkavik, E. Tangstad, Catal. Today 21 (1994) 535.
[31] J.T. Richardson, B. Turk, M.V. Twigg, Appl. Catal. A: Gen. 148 (1996) 97.
[32] J. Rynkowski, T. Paryjczak, M. Lenik, Appl. Catal. A: Gen. 106 (1993) 73.
[33] H. Jin, T. Okamoto, M. Ishida, Energy Fuels 12 (1998) 1272.
[34] R. Villa, C. Cristiani, G. Groppi, L. Lietti, P. Forzatti, U. Cornaro, S. Rossini, J. Mol. Catal. A: Chem. 204–205 (2003) 637.